Laser parameter precision diagnostic system of large-aperture high power laser experiment platform

Xia Yanwen[1], Zheng Kuixing[1], Da Zhengshang[2], Li Hongguang[2], Zhao Junpu[1], Sun Zhihong[1], Peng Zhitao[1], Wang Zhengzhou[2], Liu Hua[1], Liang Yue[1], Li Sen[1], Zheng Xiaoxia[2], Wei Xiaofeng[1]

(1. Research Center of Laser Fusion, China Academy of Engineering Physics, Mianyang 621900, China;
2. Xi′an Institute of Optics and Fine Mechanics, Chinese Academy of Sciences, Xi′an 710119, China)

Abstract: A multi-functional high-precision comprehensive diagnostic system for laser parameters was developed. The entire diagnostic system was composed of a fundamental frequency laser diagnostic module, a tripled frequency laser diagnostic module, an online optic damage inspection module, an opening frequency conversion unit and corresponding auxiliary units. Under the control of the system software, it can automatically perform accurate measurement, data collection, storage and processing on laser parameters such as near-field, far-field, energy, wavefront and pulse-waveform before and after the laser frequency conversion. This system provides accurate data for improving laser facility load capacity and researching relevant key unit technology.

Key words: laser diagnostics; pulse energy; near field; far field; high power laser
CLC number: TN247 **Document code:** A **DOI:** 10.3788/IRLA201645.1217008

大口径高通量验证实验平台的激光参数精密诊断系统

夏彦文[1],郑奎兴[1],达争尚[2],李红光[2],赵军普[1],孙志红[1],彭志涛[1],王拯洲[2],刘 华[1],梁 樾[1],李 森[1],郑小霞[2],魏晓峰[1]

(1. 中国工程物理研究院 激光聚变研究中心,四川 绵阳 621900;
2. 中国科学院西安光学精密机械研究所,陕西 西安 710119)

摘 要: 研制了多功能、高精度的激光参数精密诊断系统,整个诊断系统由基频光诊断模块、三倍频光诊断模块、在线损伤检测模块、开放式频率转换组件以及相应的辅助单元组成,在系统控制软件调度下自动完成频率转换组件前后的光束近场、远场、能量、波前和脉冲波形等激光参数的精密测量以及数据采集、储存和处理,为激光装置负载能力提升和相关关键单元技术的研究提供准确可靠的数据。

关键词: 激光诊断; 脉冲能量; 近场; 远场; 高功率激光

收稿日期:2016-04-11; **修订日期**:2016-05-10

基金项目:国家自然科学基金(61377102);国防基础科研项目(B1520133010)

作者简介:夏彦文(1972-),男,副研究员,博士,主要从事高功率激光参数诊断方面的研究。Emial:xiayanwen1972@163.com

0 Introduction

The large-aperture high power laser experiment platform can perform comprehensive verification evaluations on the load capacity of the key optical units, components and the entire system under high energy flux level[1-3]. Its laser parameter precision diagnosis system (PDS) is located at the end of the facility (Fig.1). It can comprehensively diagnose the optical properties of the output laser beam on the platform. This system provides comprehensive and accurate laser parameters to study associated scientific and technological problems on the frequency conversion components[4].

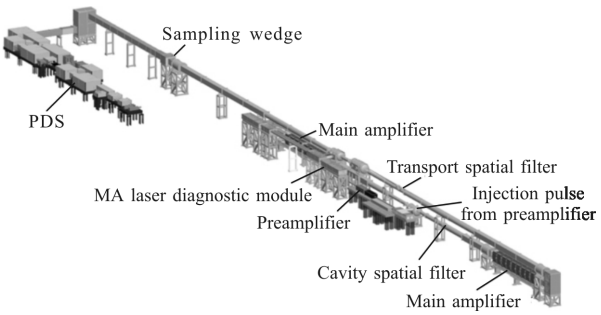

Fig.1 View of the large-aperture high power laser experiment platform

The PDS is a huge system project. Not only does it include large number of control components and detection sensors, it also includes many structural and optical interfaces, as well as interface to control system, video network, data processing system, etc. In order to lower the system cost and to improve the system operating efficiency, the system is designed under the following rules: utilize off-the-shell proven technology as much as possible to minimize any technological risks; follow the "unit-standardization, unit-modulation" rule in structural designs, and use commercial standard units, in order to improve system reliability; minimize the number of mobile plug-in whenever possible; matching precision between the measurement device configuration and the subjects being measured; when choosing between different component models, measurement precision improvement in the future and functional scalability is a top design concern; reuse alignment control and diagnosis functionality as much as possible; follow the resource sharing rules. In order to reduce the preparation work before the laser shot, the diagnosis modules on all key positions along the laser beam should independently work in segments and in parallel. This simplifies the requirement for image and data processing.

1 System functionality

The main purpose of PDS is to fully characterize the optical properties of the laser facility end output, including: laser beam energy, spatial distribution, temporal profile, the damage properties of the frequency conversion unit, etc. The entire system is divided into the following modules based on their functionalities: fundamental frequency (1ω) laser diagnostic module, tripled frequency (3ω)laser diagnostic module, opening frequency conversion unit, online optic damage inspection module, associated auxiliary system, etc. See Fig.2 for more details. In

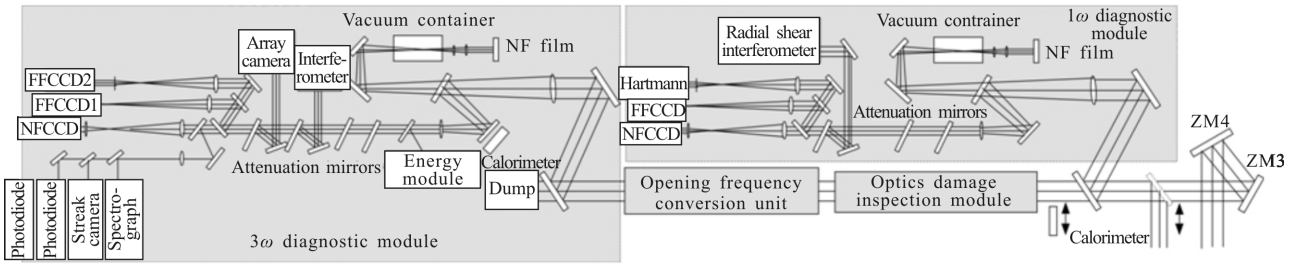

Fig.2 Top view of the laser precision diagnostic system

order to take the measurement requirement from the SG III prototype laser facility[3] into account, we add a cut-in mirror at the prototype beam entrance, and perform laser parameter comprehensive diagnosis for the prototype facility based on the functionalities with the existing diagnosis system.

2 System optical paths

The overall optical technological solution of the PDS references the set-up of the SG III laser facility and designs of similar foreign devices[5-7]. The choice of the diagnosis items is based on the functional requirement of the platform. Based on properties such as measurement functionality, structural properties and assemblies, the system can be divided into the following units: optical path docking module, energy measurement module, telescopic shrink beam module, attenuation module, near-field diagnosis module, far-field diagnosis module, etc. There is a reliable positioning structure between each module and their supporting platform, which makes online docking and maintenance of each module much easier. The diagnosis module places considerable attentions on managing the stray light, and effectively treats the remaining stray light with beam dump. The overall system optical path is illustrated in Fig.2.

The high-precision laser parameter diagnosis module samples the laser beam with spectrophotometric reflection. It uses Schlieren method to implement large dynamic-range and high-precision diagnosis on the far-field laser focal spot morphology[8]. It also uses high-speed biplanar phototube combined with high-bandwidth oscilloscope multi-channel multiplexing to implement high dynamic range measurement on pulse temporal profile[9-10]; it uses streak-camera to complete high-resolution diagnosis on pulse temporal profile; uses scientific grade CCD to complete contrast measurement of the near-field laser beam[11-12]; utilizes photosensitive recording film to perform high-precision monitoring on the laser beam near-field; employs spectrometer for spectral distribution measurement.

2.1 Fundamental frequency laser diagnostic module

Under the spatial constraints of the laser hall, the 400 mm×400 mm aperture main laser beam enters the PDS after being rotated 90° by reflection from the two vertically paired turning mirrors in the upper-left corner of Fig.1. First it enters the fundamental frequency (1ω) laser diagnostic module, as illustrated in Fig.2: the incident beam is rotated another 90° by the two planar mirrors ZM4 and ZM3 before it enters the diagnosis platform. ZM4 is a large aperture distorting mirror. Its beam angle of incidence is 22.5°, which aims to minimize the size of the distorting mirror. It is used in combination with the Hartmann sensor internal to the diagnosis module, which can be used to improve the main laser beam quality. The laser beam undergoes Fresnel reflection sampling by two 1ω sampling mirror, before it enters the large aperture shrink-beam system, a Galilean telescope. In order to ensure the transmitted wave-front, the 1ω shrink beam lens is a coaxially rotationally symmetric ellipsoid lens. We insert a mirror in the shrink-beam system, where the transmitted light enters the high-resolution near-field diagnosis components, and the reflected light enters other diagnosis modules. Therefore the same 1ω shrink-beam lens is shared between the 1ω high-resolution near-field optical path and other 1ω measurement paths. This reduces the spatial requirement of the system and its complexity. The large aperture shrink-beam system shrinks the main laser beam to 50 mm×50 mm, before it passes the attenuation module and splitting module that follow, and then enters the 1ω near-field alignment module, wave-front measurement module, far-field diagnosis module. The attenuation module is composed of three coated wedges, each of which is divided into two segments, and each segment is coated separately. Through adjusting the appropriate gear for 1ω attention wedges 1,2,3, we can fit the system under different energy match requirements under both the laser alignment and shot stage. It ensures the laser energy is well positioned within the dynamic range of

the sensors.

The high-precision 1ω near-field measurement optical path is based on a combination of positive-positive lens, in order to transfer the near-field image to the sensor unit. The image size is 50 mm×50 mm, and is measured with high-precision on the near-field using films. The optical resolution is 0.7 mm. Because it demands quite large amount of energy, to avoid any breakdown at the real focal point, the focal spot area is placed within a vacuum container.

The near-field alignment optical path is also based on the combination of positive-positive lens in a similar fashion. A 50 mm×50 mm light beam passes a convergent lens and a 1ω collimated lens, and becomes an 8 mm×8 mm light beam. In order to meet near-field light beam alignment accuracy requirement of 0.5% at the output, the near-field CCD pixel size is required to be no more than 30 μm, and the target surface size is no less than 12 mm×12 mm. Therefore, we use a scientific grade CCD with a pixel size of 13 μm and a target surface of 13 mm×13 mm as the sensor unit.

The 1ω far-field alignment chooses a system focal distance f'=9 126 mm. To meet the far-field alignment accuracy requirement of 2.5 μrad, we choose a CCD with pixel size of 4.65 μm, and a target surface size of 6.4 mm×4.8 mm as the sensor unit.

At the entrance of each sensor, there are fixed filters and attenuation wheels. The fixed filters are used to eliminate stray light. Through different combinations of attenuation wheels and attenuation wedges, we can control the incident energy within a range reasonable for measurement.

2.2 Tripled frequency laser diagnosis module

As illustrated in Fig.2, after the opening frequency conversion module, the light transmitted from the first 1ω sampling mirror is converted to a mixed light composed of 1ω, second harmonics (2ω) and tripled harmonics (3ω). After being sampled by Fresnel reflection at the two 3ω sampling mirrors, the mixed light enters a large aperture 3ω shrink beam system, which shrinks the light beam aperture from 400 mm× 400 mm to 50 mm×50 mm. After passing through the attenuation module and the spliting module that follow, the light enters various 3ω diagnosis modularized optical paths. This completes the relevant functional measurement on the 3ω sub-system. The mixed light passes through the first 3ω sampling mirror and enters the absorber. The entrance of the absorber is equipped with an interface to a large aperture energy meter(calorimeter), which can be used to measure the total energy of the third harmonics when necessary.

Similar to the 1ω diagnosis module, the large aperture 3ω shrink beam system is a Galilean telescope. It is shared between the 3ω near-field high-resolution optical paths and other 3ω measurement optical paths. However, four attenuation wedges are used here. The third attenuation wedge is used to measure the wave-front distortion of the reflected light. The fourth attenuation wedge is used to measure the dynamic focal surface of the reflected light. The light coming of the fourth attenuation wedge is divided into four groups by the splitter, and enters focal spot side-lobe, the main lobe, near field, temporal and spectral measurement optical path, respectively.

In the 3ω near-field low-resolution measurement, we use a Kepler telescope system to shrink the light into an 8 mm×8 mm beam. The optical resolution is 2 mm. The focal spot tests are divided into “main lobe” and “side lobe” tests. The optical path of the main lobe tests uses CCD camera to measure the microscopically magnified main lobe morphology. At the focal plane in the side lobe measurement optical path, we place a Schlieren device, which can block the laser from the main lobe and measure the side lobe. With the focal spot images separately collected from the main and the side lobe, we use relevant algorithm to reconstruct the focal spot, and therefore attain the complete laser focal spot morphology. In order to meet the device requirement under different

experiment circumstances, we divide the side lobe focal spot measurement range into a large and small field of view gear positions. Based on the actual laser quality in the experiment, one of the two gear positions will be used.

Through the focal spot changes in the dynamic focal plane measurement optical path monitoring device under both the high and low energy shots, we can determine the wave-front distortion from the facility output, with the assistance of array cameras, recorded by films.

The PDS incorporates four calorimeters, all of which are located behind the frequency conversion crystals. They are used to measure the energy of the remaining 1ω light, remaining 2ω light, and 3ω laser light, as well as the three-wavelength sampling energy for the purpose of energy rebalance.

The total energy is sampled by transmission at the 3ω near field local reflection mirror 2 in the large aperture 3ω shrink-beam system. The energy in the monochromatic light is sampled by reflection at the dichroic mirror in front of the first attenuation wedge. After it is filtered by a monochrome filter, the light enters 1ω, 2ω and 3ω calorimeter, respectively. See Fig.3 for illustration.

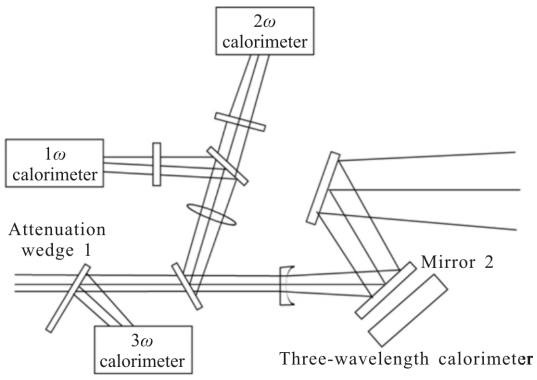

Fig.3 Energy measurement modules

It is the energy after the crystal that is measured by the single wavelength energy meter. The energy rebalance refers to the fact that the readings from the three-wavelength calorimeter, W_4, maintain a constant quantitative relationship with the readings from the single wavelength calorimeter. That relationship can be used to check whether the energy sampling coefficients in the various single wavelength calorimeter remain constant. The energy before the crystal, E_{in}, is derived from the master amplifier calorimeter. The third harmonics conversion efficiency of the crystal, η, is given by the ratio between the tripled harmonics energy, $E_{3\omega}$, and the energy before the crystal, E_{in}. Their respective relationships are given as follows:

$$E_{out}=\sum_{i=1}^{3}E_{i\omega},\ E_{i\omega}=K_iW_i,\ W_4=\sum_{i=1}^{3}h_iW_i$$

Here E_{out} is total energy after the crystal; $E_{i\omega}(i=1,2,3)$ refers to the corresponding single wavelength energy; K_i is the energy sampling coefficients of the corresponding single wavelength calorimeter; W_i refers to the readings from the single wavelength calorimeter; h_i is the balance factor of the energy meters[13].

In order to eliminate the stray light effectively, we employ multiple strategies. For reflection units, we place absorbers for the transmitted light; for transmission unit, we also use absorbers in the direction of stray reflection light; the attenuation optical unit is built in the form of wedges, to avoid the influence of multiple reflected stray light; trace residue reflection at the surfaces of every optics element, to eliminate the ghost spot influence on the optical path; we also employ diaphragm to eliminate stray light at the convergent focal spot; at the same time, we blacken the surface of all structural components within the measuring module, to further reduce the influence of the stray light.

3 System structures

The area for the overall structure of the PDS is about 22 m×3 m. Based on the requirement from the main optical path docking and operations, the overall height of the optical axis as a whole is 1.226 m, and the total height is 1.656 m. The PDS can be divided

into many modules based on functionalities. Because the provided space for the system is long and narrow, all the modules employ optical platform support. The module enclosures are sealed with the countertops, all the module enclosures are connected with pipes, and all the enclosures employ a removable structure connected by frameworks and sealed by plates. When the components require maintenance, the covers can be directly removed, and makes the process quick and easy.

4 System debugging

First, we use EX250, a 32-channel vibration mode testing system, to test the stability of this work platform. The testing result shows that the dynamic response acceleration of the optical platform from the environmental stimulus has a RMS on the order of magnitude of 10^{-4} m/s^2, the displacement RMS value has an order of magnitude of 10^{-8}–10^{-7} m, and the acceleration power spectrum has an average value on the order of magnitude of 10^{-11}–10^{-10} g^2/Hz (the foundation platform in the high-power solid laser facility has a design specification of 10^{-10} g^2/Hz). The test results show that under the circumstances where the environmental stimulus mostly come from HVAC, local fans and occasional stimulus, the laser parameter precision diagnosis platform has an excellent stability. Figure 4 shows the power spectrum of the optical platform along the x-axis.

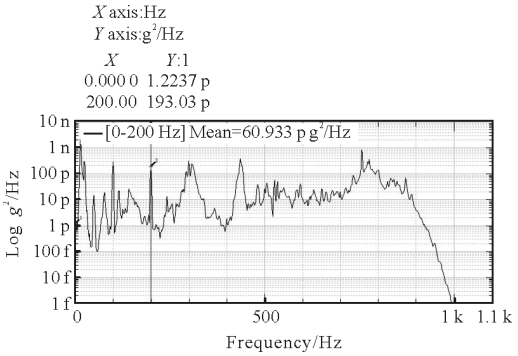

Fig.4 Power spectrum of the optical platform along the x-axis

In order to understand the overall performance of the 1ω diagnosis module, we employ a back-tracing approach: a standard wave-front optical fiber laser is used as standard light source. It is placed at the entrance to the far-field CCD camera, and transfer light beam backward. A large aperture reflection mirror is placed in front of the 1ω shrink-beam lens. After being reflected by this mirror, the light reenters the optical paths into the near-field CCD and Hartmann wave-front CCD to obtain the near-field and wavefront data. Therefore the data we collect result from that the standard light source passes through the optical paths twice.

Since the 3ω module has a relatively large attenuation, also that our current 3ω optical fiber light source does not have a sufficient power, we cannot use the same back-tracing approach. Therefore we utilize the 1ω shrink-beam lens, and form a large aperture parallel light tube with the pairing lens in front of the standard light source: a standard wave-front laser with a wavelength of 351 nm passes through the laser pairing lens before it enters the 1ω shrink-beam lens. After that, the laser becomes a 400 mm×400 mm large caliber parallel light beam. This light beam enters the 3ω diagnosis module to complete the test on module specifications.

The inhomogeneity with the 351 nm light source leads to the uneven distribution within the near field image. This significantly affects the modulation and contrast measurement of the 3ω diagnostic module. Therefore we employ an image mosaic method to take 49 images in total. Only the relatively even part of each image is taken. All the sub-images are combined into an even near-field image to complete the measurement.

The diagnostic capabilities of PDS are listed as in Tab.1.

During the system debugging stage for the precision diagnosis, we compare the images from the 1ω diagnosis module and those from the 3ω diagnosis module under the same shot. As illustrated in Fig.5, the comparison shows that the main outlines as well as the locations of multiple defects are the same

between the two images. This implies that the data and images measured by the diagnosis system are trustworthy.

Tab.1 Diagnosis capability of the laser precision diagnostic system

Diagnosis items		Diagnostic capabilities	
		Infrared (λ=1 053 nm)	Ultraviolet (λ=351 nm)
Far field	Far-field imaging FOV	10−30 DL	30−120 DL
	Dynamic range	~100:1	~1000:1
	Resolution	~3 DL	~3 DL
Wavefront aberration		$P-V$<0.7 λ	$P-V$<2.1 λ
Near field	Imaging resolution	0.7 mm	2 mm
	Dynamic range	~100:1	~100:1
	Modulate(M)	~1.17	M<1.2
	Contrast(C)	0.06	0.04
Temporal profile	Dynamic range	~100:1 (VPD+OSC)	~100:1 (VPD+OSC)
	Rise time (10%−90%)	~90 ps (VPD+OSC)	~90 ps (VPD+OSC)
	Resolution	~10 ps (streak camera)	~10 ps (streak camera)
Wavelength	Resolution	0.02 nm	0.02 nm
Dynamic focus plane	Longitudinal resolution	10 μm	10 μm
Alignment	NF alignment accuracy	0.5%of the aperture	0.5% of the aperture
	FF alignment accuracy	~2.5 μrad	~2.5 μrad
Pulse energy	Range	1−18 kJ	0.5−14 kJ
	Accuracy	4.0%	4.0%

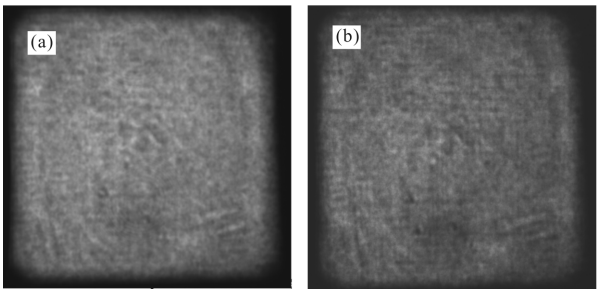

Fig.5 1ω near-field (a) and 3ω near-field (b) images

Since the frequency conversion components do not incorporate focusing lens, we cannot use traditional approaches to directly quantify the energy sampling coefficients of the calorimeters. Instead, we employ combinational indirect measurement. This will take more than ten laser shootings. Then we utilize linear regression, and minimize the least square in the linear combination to obtain the sampling parameters.

Figure 6 gives the relationship curve between the synthesis energy $(E_{1\omega}+E_{2\omega}+E_{3\omega})$ and the experimental results after the crystal, as well as the relationship between the combined $(h_1W_1+h_2W_2+h_3W_3)$ and the measured three-wavelength calorimeter reading used for energy balance, W_4. From this figure, we can see that the relative error between the synthesis and measured after-crystal energy is with 1%, and the relative error between the synthesis and the measured three-wavelength energy meter readings used for energy balance is within 0.2%.

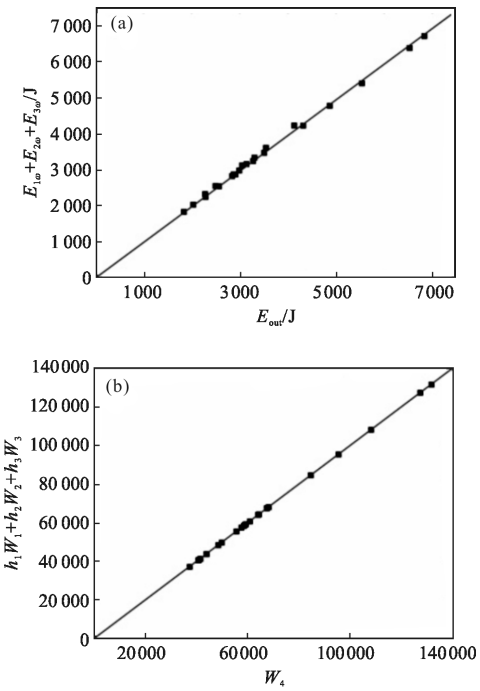

Fig.6 Experimental and synthetic energies results relationship curves

5 Conclusion

We developed a multi-function high-precision laser parameter diagnosis platform. This system can

give the laser parameter information before and after the main laser beam is frequency converted. The online control and the sub-station control to the PDS have been under normal operations. The preparation time for the measurement system is about 5 minutes, the data collection time is about 2 minutes, and the central processing time for the data is about 1 minute. During the debugging process, we had discovered that due to the lower power in the 3ω analogue light source, the Schlieren collimation of the 3ω focal spots is quite difficult. Therefore we will take the transfer problem of the collimated light source into consideration, as part of our future works. We did not discuss opening frequency conversion modules and the online optic damage inspection module here. We will elaborate them in future publications.

References:

[1] Haynam C A, Wegner P J, Auerbach J M, et al. National ignition facility laser performance status [J]. ***Applied Optics***, 2007, 46(16): 3276-3303.

[2] Burkhart S C, Behrendt W C, Smith I. Beamlet laser diagnostics[R]. UCRL-LR-105821- 95-1.

[3] Zhang Xiaoming, Zheng Wanguo, Wei Xiaofeng, et al. Preliminary experimental results of Shenguang Ⅲ technical integration experiment line[C]//SPIE, 2005, 5627: 6-12.

[4] Conder A, Alger T, Azevedo S, et al. Final optics damage inspection(FODI)for the national ignition facility[R]. UCRL-PROC-236458, 2007.

[5] Noel Fleurot, Claude Cavailler, Bourgade J L. The Laser M′egajoule (LMJ) project dedicated to inertial confinement fusion: Development and construction status [J]. ***Fusion Engineering and Design***, 2005, 74: 147-154.

[6] Kegelmeyer L M, Raelyn Clark, Richard R Leach Jr, et al, Automated optics inspection analysis for NIF [J]. ***Fusion Engineering and Design***, 2012, 87: 2120-2124.

[7] Wegner Paul J, Van Wonterghem Bruno M, Dixit Sham N, et al. Characterization of third-harmonic target plan and irradiance on the nation ignition facility beamlet demonstration project[R]. UCRL-JC-123070, 1996.

[8] Thompson C E, Decker D E, Knopp C F. Optics damage inspection for the NIF[R]. UCRL-JC-130034, 1998.

[9] Leclerc P, Allouche V. Temporal response diagnostic for the laser MègaJoule[C]//SPIE, 1999, 3492: 843-850.

[10] Thomas S, Boyd B, Davis D T, et al. Temporal multiplexing for economical measurement of power versus time on NIF [C]//SPIE, 1997, 3047: 700-706.

[11] Sun Zhihong, Peng Zhitao, Liu Hua, et al. Calculated methods of high power laser near field parameters [J]. ***Chinese Journal of Lasers***, 2008, 35(4): 544-548

[12] Zhao Junpu, Hu Dongxia, Zhou Wei, et al. Analysis of near-field power spectral density in high-power solid-state laser [J]. ***Acta Optica Sinica***, 2008, 28: 118-122

[13] Xia Yanwen, Liang Yue, Li Sen, et al. Energy measurement system of a large-aperture high power laser experiment platform [J]. ***High Power Laser Science and Engineering***, 2013, 1(3-4): 126-131.